

Structure and Dynamics of CTX-M Enzymes Reveal Insights into Substrate Accommodation by Extended-spectrum β -Lactamases

Julien Delmas^{1,2}, Yu Chen³, Fabio Prati⁴, Frédéric Robin^{1,2}, Brian K. Shoichet³ and Richard Bonnet^{1,2*}

¹Laboratoire de Bactériologie, CHU Clermont-Ferrand, Clermont-Ferrand F-63003, France

²Laboratoire de Bactériologie, UFR Médecine, Université Clermont1, EA3844, Clermont-Ferrand F-63001, France

³Department of Pharmaceutical Chemistry, University of California, San Francisco, QB3 Building Room 508D, 1700 4th Street, San Francisco, California 94143-2550, USA

⁴Department of Chemistry, Università di Modena e Reggio Emilia, via Campi 183, Modena, Italy

Received 8 August 2007;
received in revised form
8 October 2007;
accepted 10 October 2007
Available online
16 October 2007

Edited by M. Guss

Oxyimino-cephalosporin antibiotics, such as ceftazidime, escape the hydrolytic activity of most bacterial β -lactamases. Their widespread use prompted the emergence of the extended-spectrum β -lactamases CTX-Ms, which have become highly prevalent. The C7 β -amino thiazol-oxyimino-amide side chain of ceftazidime has a protective effect against most CTX-M β -lactamases. However, Asp240Gly CTX-M derivatives demonstrate enhanced hydrolytic activity against this compound. In this work, we present the crystallographic structures of Asp240Gly-harboring enzyme CTX-M-16 in complex with ceftazidime-like glycyboronic acid (resolution 1.80 Å) and molecular dynamics simulations of the corresponding acyl-enzyme complex. These experiments revealed breathing motions of CTX-M enzymes and the role of the substitution Asp240Gly in the accommodation of ceftazidime. The substitution Asp240Gly resulted in insertion of the C7 β side chain of ceftazidime deep in the catalytic pocket and orchestrated motions of the active serine Ser70, the β 3 strand and the omega loop, which favored the key interactions of the residues 237 and 235 with ceftazidime.

© 2007 Elsevier Ltd. All rights reserved.

Keywords: β -lactamases; ceftazidime; CTX-M; spectrum; structure

Introduction

The production of β -lactamases is the predominant cause of resistance to β -lactam antibiotics in Gram-negative bacteria. Oxyimino-cephalosporins such as ceftazidime and cefotaxime escape the hydrolytic activity of most β -lactamases. These β -lactams harbor bulky C7 β aminothiazol-oxyimino-amide side chains that make them inher-

ently less susceptible to β -lactamases. The methyl function of the cefotaxime oxyimino group is replaced by a carboxypropyl function in ceftazidime (Fig. 1a). Unfortunately, their widespread use prompted the emergence of extended-spectrum β -lactamases (ESBLs). These enzymes confer resistance to oxyimino-cephalosporins and lead to poor clinical outcomes. Before 2000, most ESBLs were derived from penicillinases, such as TEM-1 or SHV-1, by point substitutions. In these ESBLs, the substitutions displace two major walls of catalytic pocket, the β 3 strand or the omega loop, and lead to an enlarged active site, which is able to recognize the large aminothiazol-oxyimino-cephalosporins.^{1,2}

*Corresponding author. E-mail address:

rbonnet@chu-clermontferrand.fr.

Abbreviations used: ESBL, extended-spectrum β -lactamase; MDS, molecular dynamics simulation.

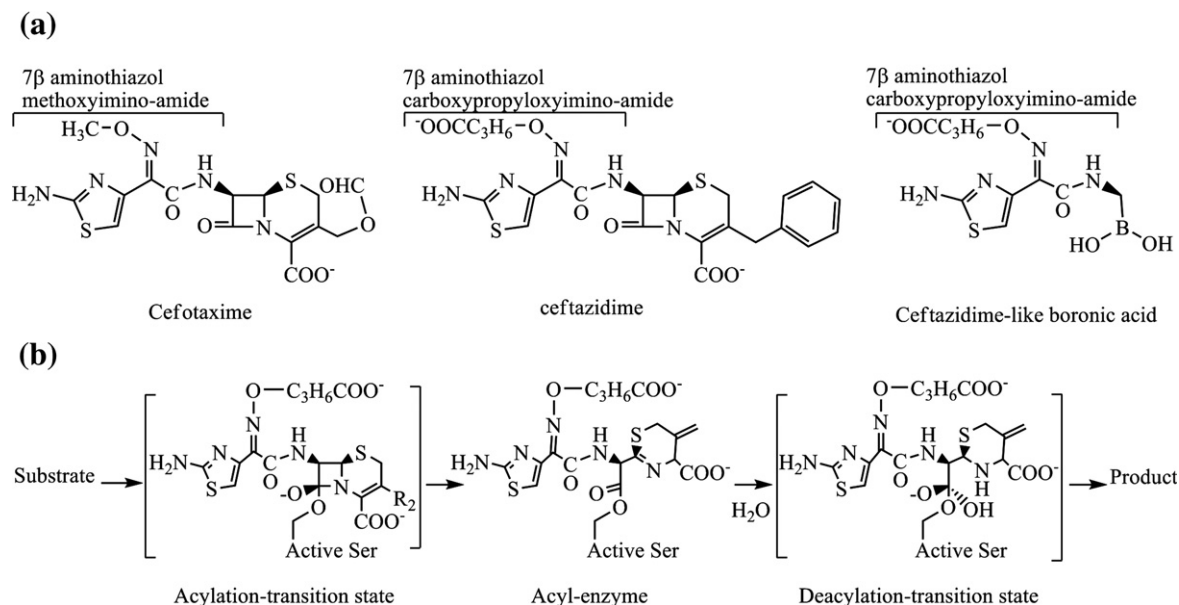


Fig. 1. Characteristics of β -lactams and the reaction cycle of serine β -lactamases. (a) Aminothiazol-oxymino β -lactam antibiotics and the ceftazidime-like glycyboronic acid. (b) The basic reaction pathway is shown with the acylation and deacylation transition states.

In 1995, CTX-M enzymes, a new group of ESBLs, emerged worldwide and are now the most frequently observed ESBLs.³ CTX-M enzymes share less than 40% identity with TEM- and SHV-type enzymes. They differ from most TEM and SHV ESBLs by a much greater hydrolytic activity against cefotaxime than against ceftazidime. However, Gly240-harboring CTX-M enzymes exhibit an unusually high activity against ceftazidime. CTX-M-16, which derives from CTX-M-9 by the substitution Asp240Gly, exhibits a 10-fold higher catalytic efficiency against ceftazidime ($k_{\text{cat}}/K_{\text{M}}$ 0.043 *versus* 0.004 $\mu\text{M}^{-1} \text{s}^{-1}$) than CTX-M-9.³ Unlike the well-studied TEM and SHV enzymes, there have been few structural studies of the CTX-M family.^{4–9} The surprising feature of CTX-M structures is that the active site is not enlarged.

ESBLs such as CTX-Ms use a reactive serine (Ser70), a catalytic water molecule and the activator residue Glu166 to hydrolyze the β -lactam ring by an acid–base catalytic mechanism (Fig. 1b).^{2,10–14} Glycyboronic acid-based compounds are useful for probing substrate recognition in that they are reversible inhibitors of CTX-M β -lactamases and bind to such β -lactamases as acylation transition-state analogs (step 2, Fig. 1b).⁹

We obtained the X-ray structure of the CTX-M-9 in complex with a ceftazidime-like boronic acid,⁹ which bears the C7 β aminothiazol-oxymino-amide side chain of ceftazidime (Fig. 1a). The derivative CTX-M-16 was four-fold more susceptible (K_i 4 *versus* 15 nM) than CTX-M-9 to this ceftazidime analogue inhibitor.⁹ To investigate this behavior, in this present study we determined the X-ray structure of CTX-M-16 in

complex with ceftazidime-like boronic acid. The acyl–enzyme structures of CTX-M-9 and CTX-M-16 in complex with ceftazidime were then modeled from these crystallographic structures and analyzed by molecular dynamics simulations (MDSs). The results provided insight into the recognition of aminothiazol-oxymino cephalosporins and the enzymatic dynamics.

Table 1. Data processing and crystallographic refinement statistics for CTX-M-16 crystal structure in complex with ceftazidime-like boronic acid

Cell constants	$a=45.12 \text{ \AA}$ $b=106.66 \text{ \AA}$ $c=47.76 \text{ \AA}$ $\beta=102.14^\circ$
Resolution (\AA)	1.80 (1.86–1.80) ^a
Total reflections	112,493
Unique reflections	37,585
R_{merge} (%)	6.6 (29.81) ^b
Completeness (%)	94.3 (87.6) ^b
$[I]/[\sigma(I)]$ ($^\circ$)	7.9 (2.1) ^b
Resolution range for refinement	10–1.80
No. of protein residues	524
No. of water molecules	897
RMSD	
Bond lengths (\AA)	0.010
Angle (deg.)	1.55
R -factor (%)	14.6
R_{free} (%) ^c	20.0
Average B -factor	
Protein	8.45
Compound	18.92
Water molecules	23.01

^a Value in parentheses is for the highest resolution shell used in refinement.

^b Values in parentheses are for the highest resolution shell information used in refinement.

^c R_{free} was calculated with 5% of reflexions set aside randomly.

Results

Overall structure of CTX-M-9 and CTX-M-16 complexes

The crystal structure of CTX-M-16 was determined in complex with a ceftazidime-like glycyboronic acid to a resolution of 1.80 Å. CTX-M-16 complex crystallized in space group $P2_1$ with two molecules per asymmetric unit as observed for CTX-M-9.⁹ The structure was solved by molecular replacement, with the structure of CTX-M-9 as a search model.⁸ The final R -factor and R_{free} values of the refined structure were 14.6 and 20.0%, respectively (Table 1). Excluding proline and glycine, 91.2% of residues were in the favored region and 8.8% were in the allowed region of the Ramachandran plot. The RMSD of the C^α position was 0.28 Å between the two monomers of the crystallographic asymmetric unit. Each monomer varies from 0.14 to 0.32 Å from the CTX-M-16 complex to the CTX-M-9 complex.⁹ The backbone structure of complexes resembled one another

closely and consisted of two domains, an α/β domain and an α domain, with the active site situated in a groove between the two domains (Fig. 2), as seen for the other class A β -lactamases.^{1,2}

The conserved element number 1 of class A enzymes (Ser70-Xxx-Xxx-Lys73) contained the active serine Ser70 and one helix–turn downstream Lys73, which both pointed at the bottom of the active site (Fig. 2). The element number 2 (Ser130-Asp131-Asn132) was situated on a short loop in the all alpha domain, where it formed one side of the catalytic cavity. On the same side, the residues Asn104 and Tyr105 formed a bend in the binding site. The conserved element number 3 (Lys234-Thr235-Gly236) was situated on the β 3 strand of a β -sheet in the α/β domain and formed the opposite wall of the catalytic cavity. The element number 4 (Glu166-Pro167-Thr168-Leu169-Asn170) was situated on a 19-residue loop (positions 161 to 179), usually referred to as the omega loop, which constituted the floor of the active site (Fig. 2).

The major electrostatic interactions between conserved elements of the catalytic pocket were similar

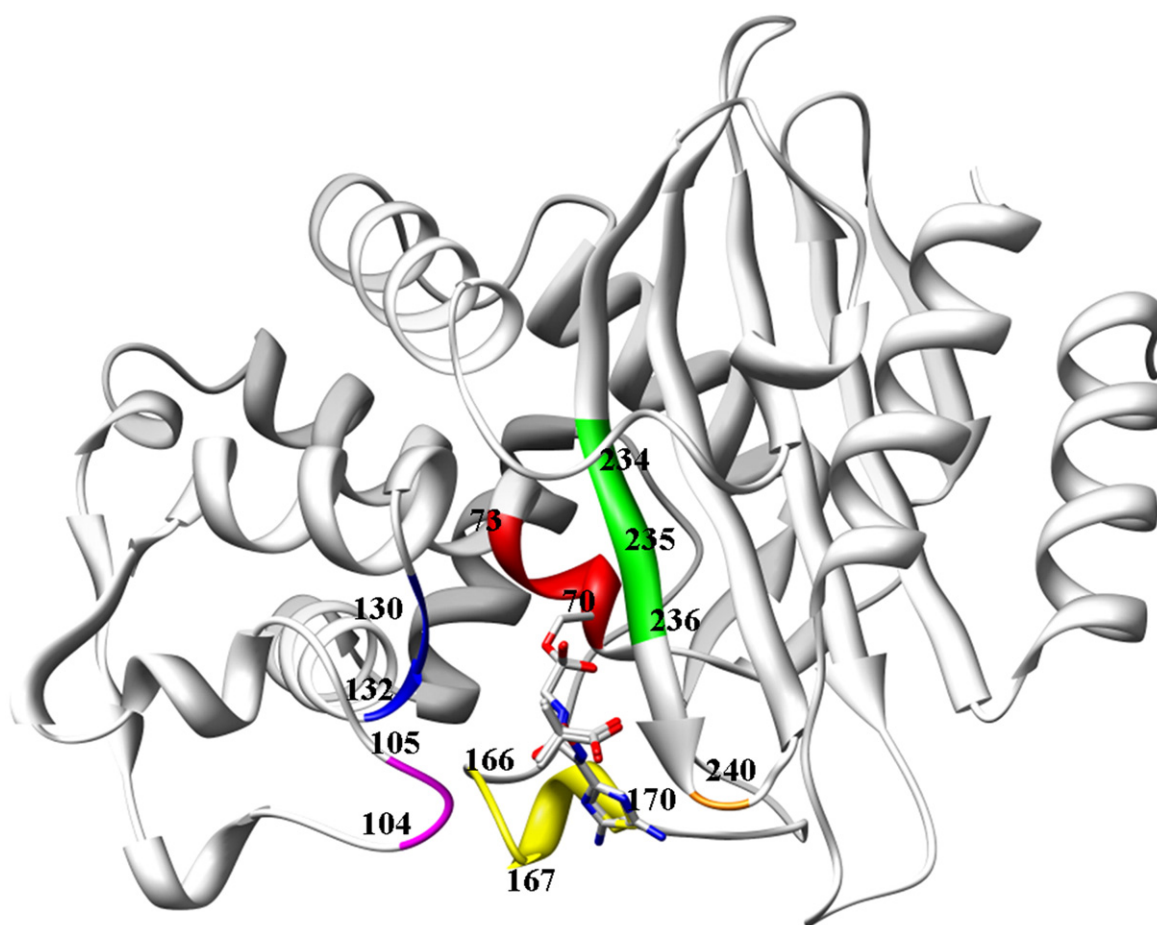
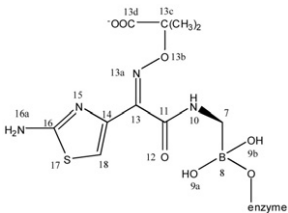


Fig. 2. Overall structure of CTX-M-9 in complex with the ceftazidime-like boronic acid compound. The conserved element number 1 (S70 to K73) of the active site is in red; the conserved element number 2 (S130-D131-N132) is in blue; the conserved element number 3 (K234-T235-G236) is in green; the residues E166 to N170 (conserved element number 4) of the omega loop are in yellow; the residues 104 and 105 are in purple; and the residue 240 is in orange. The compound and the catalytic Ser70 are shown as a stick model with grey carbon atoms, red oxygen atoms, and blue nitrogen atoms.

Table 2. Key interactions in the complex structures

Complexes	CTXM-9 ^a	CTXM-16
Numbering of compound atoms		
<i>Distance between key residues of the binding site^b</i>		
Catalytic water–S70 O ^γ	2.71, 2.69	2.81/2.62, 2.68/2.68
Catalytic water–E166 O ^{ε2}	2.56, 2.53	2.54, 2.44
Catalytic water–N170 N ^δ	2.72, 2.73	2.68, 2.79
K73 N ^ε –S70 O ^γ	3.21, 3.08	3.01/3.13, 2.95/2.95
K73 N ^ε –E166 O ^{ε2}	4.21, 4.13	4.09, 4.00
K73 N ^ε –N132 O ^{δ1}	2.72, 2.69	2.78, 2.69
K73 N ^ε –S130 O ^γ	2.93, 2.86	2.91, 2.84
K234 N ^ε –S130 O ^γ	2.84, 2.87	2.82, 3.01
<i>Distance between key residues of the binding site and compound atoms^b</i>		
S70N–O9a	2.84, 2.79	2.78/2.80, 2.83/2.86
S237N–O9a	2.75, 2.77	2.84/2.75, 2.81/2.76
S237O–O9a	2.75, 2.73	2.78/2.83, 2.68/2.69
S130O ^γ –O9b	2.71, 2.70	2.80/2.81, 2.75/2.77
S237O–NH10	3.39, 3.36	3.29/3.41, 3.19/3.32
S237O ^γ –NH10	3.15, 3.13	3.33/3.34, 3.41/3.45
S237O ^γ –O13b	3.49, 3.33	3.31/3.35, 3.30/3.13
S237O ^γ –COO ⁻ 13d	2.83, 2.73	2.99/3.15, 3.09/3.25
N132N ^{δ2} –O12	2.84, 2.77	2.70/2.72, 2.63/2.65
N104N ^{δ2} –O12	2.98, 2.95	3.06/2.92, 3.04/2.98
D240O ^{δ1} –N16a	2.83, 2.84	Not possible

^a From Ref. 9.

^b Two distances in monomers A and B. In cases with two distances shown within one monomer, multiple conformations are present.

in CTX-M-9 and CTX-M-16 complexes (Table 2). The two residues Glu166 and Asn170 established a hydrogen network with the catalytic water molecule. The N^ε atom of Lys73 in conserved element 1 was located at hydrogen-bond distance of Ser130 and Asn132 side chains of the conserved element number 2. Lys234 and Ser130 side chains formed a hydrogen bond that connected the α/β and the α domains. These interactions were previously observed in the CTX-M-9 and CTX-M-16 apoenzymes and other class A enzymes.⁸ Ceftazidime-like boronic acid binding thus did not induce major structural changes in the CTX-M-9 and CTX-M-16 enzymes.

Interaction of ceftazidime-like compound with the CTX-M binding sites

The position of the ceftazidime-like compound in the active site of CTX-M-16 was unambiguously identified in the initial $F_o - F_c$ electron density difference map contoured at 2σ (Fig. 3). The glycyboronic acid adopted a conformation in the active site consistent with a tetrahedral acylation transition state, as previously observed in TEM-1 and CTX-M-9 boronic acid structures.^{9,15} Electron density connected the O^γ of the catalytic Ser70 to the boron

atom of the glycyboronic acid. At the top of the binding site, the boronic acid hydroxyl O9b interacted with O^γ of the Ser130, and the O9a boronic acid hydroxyl hydrogen bonded with the N backbone atoms of residues 70 and 237, which form the “oxyanion” hole of class A enzymes¹⁶ (Table 2, Fig. 4). The O12 atom of the amide group was hydrogen-bonded with N^{δ2} atoms of Asn132 and Asn104 (Table 2, Fig. 4). The aminothiazol ring of the compound pointed towards the omega loop and the oxyimino group lay in the vicinity of the $\beta 3$ strand, as previously observed with CTX-M-9 in complex with ceftazidime-like boronic acid and in the acyl–enzyme structure of the CTX-M enzyme Toho-1 in complex with cefotaxime.^{5,9} These data suggested that the compound mimics the aminothiazol-oxyimino-amide group of cephalosporins.

However, CTX-M-9 and CTX-M-16 complexes exhibited different features. In the CTX-M-9 complex, the carboxyl group of Asp240 hydrogen-bonded with the amino group of the aminothiazole ring, as observed in the cefotaxime acyl–enzyme complex of Toho-1.^{5,9} This interaction was absent in the Gly240-harboring enzyme CTX-M-16 and the aminothiazole ring adopted a double conformation. The two conformations have similar occupancies. In conformation 1, the amino group of the aminothiazole ring was directed towards the solvent, as observed with the CTX-M-9 complex. In conformation 2, the amino group of the aminothiazole ring pointed towards the residue Pro167 of the omega loop (Figs. 3 and 4).

The substitution Asp240Gly of CTX-M-16 was also associated with different electrostatic interactions for the carboxypropyl function of the ceftazidime-like compound. In the CTX-M-16 complex, this function only interacted with the O^γ atom of Ser237. The Arg276 side chain pointed away from the

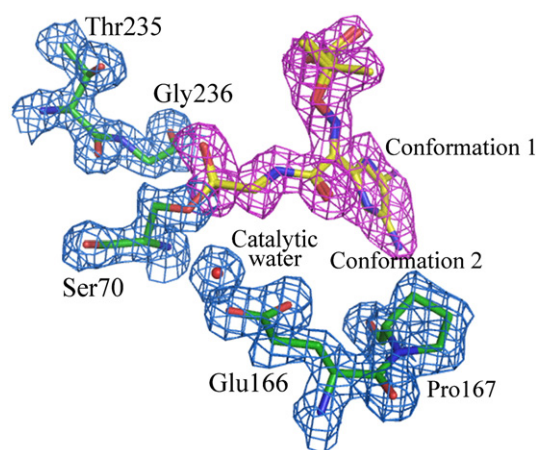


Fig. 3. Active-site electron density for CTX-M-16 complex structure. The $2F_o - F_c$ electronic density of the refined model of CTX-M-16, contoured at 1σ , is shown in green, and the simulated-annealing omit electron density of the ligand, contoured at 2σ , is shown in purple. Carbon atoms are in green for the protein or in yellow for the adduct; oxygen atoms are red, and nitrogen atoms are blue. The conformations of the compound are indicated as conformation 1 and conformation 2.

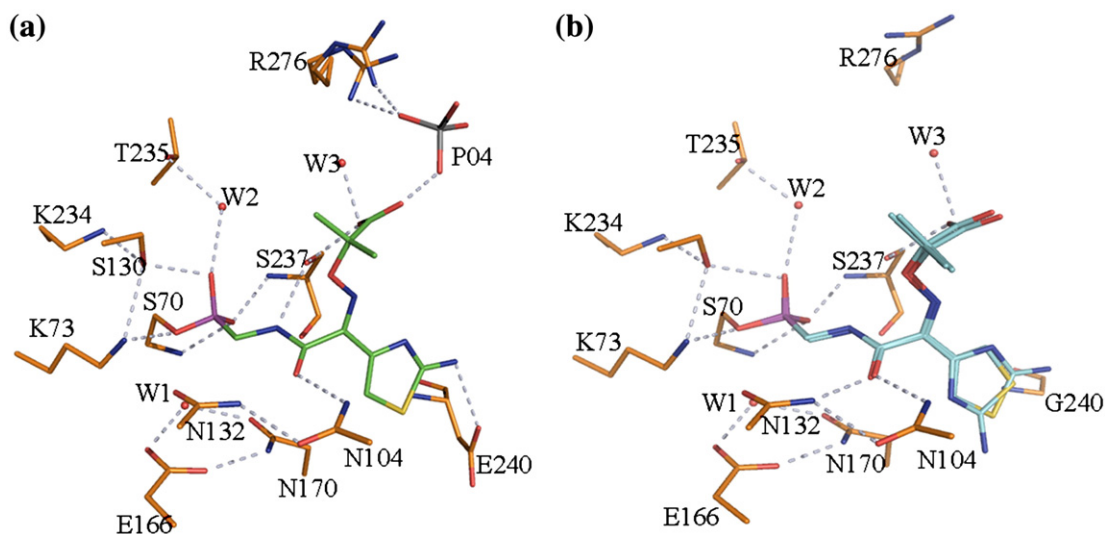


Fig. 4. Key polar interactions observed between CTX-M-9 (4A)⁹ or CTX-M-16 (4B) and the ceftazidime-like glycylicboronic acid. Carbon atoms are in yellow for the protein or in green for the adduct; oxygen atoms are red, and nitrogen atoms are blue.

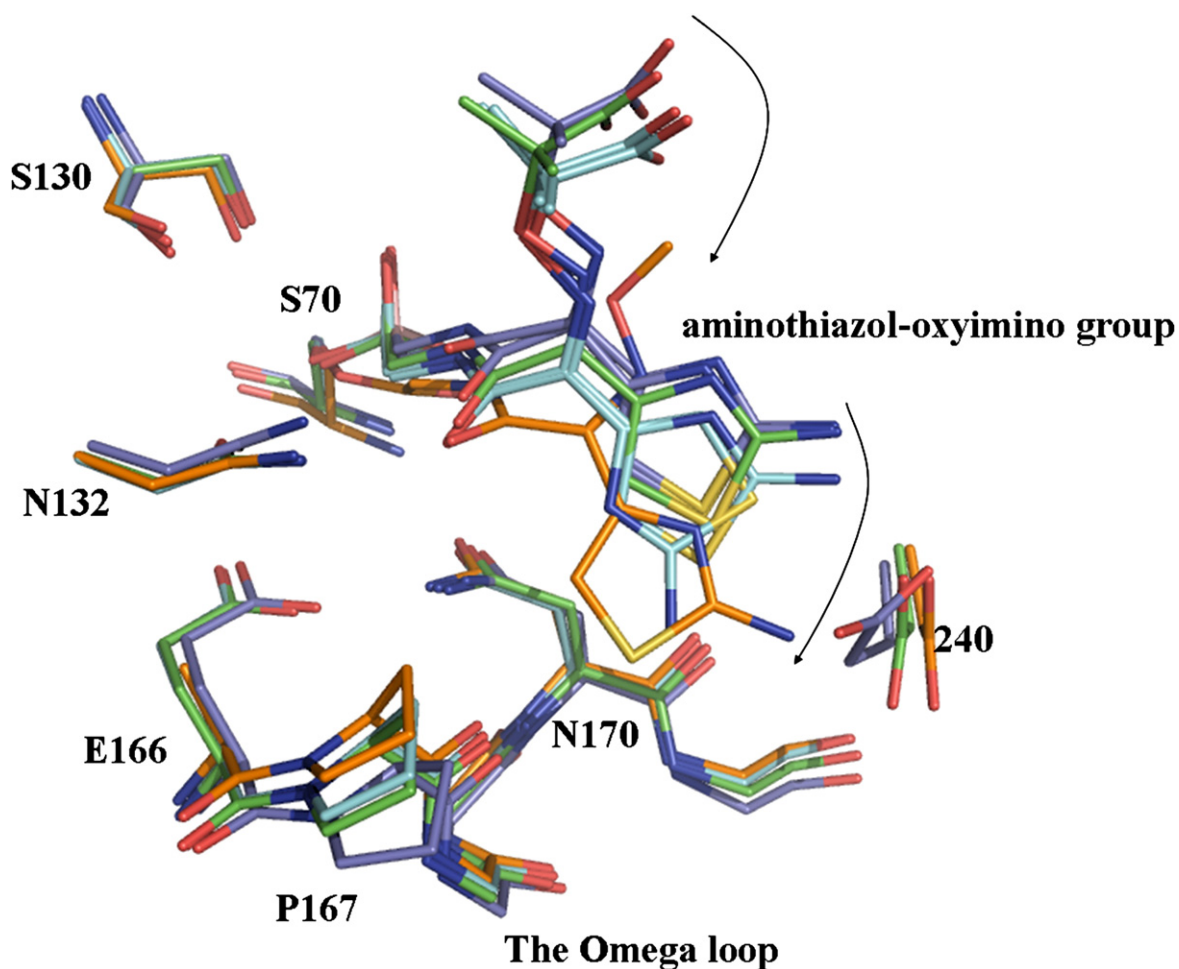


Fig. 5. Superimposition of CTX-M-9 and CTX-M-16 complexes with TEM-1 structure in complex with the ceftazidime-like glycylicboronic and cefotaxime acyl-enzyme structure of Toho-1.^{5,9,12} Carbon atoms are in cyan for the CTX-M-16 complex, in green for the CTX-M-9 complex, in orange for the Toho-1 complex and in blue for the TEM-1 complex; oxygen atoms are in red, nitrogen atoms in blue, boron atoms in purple and phosphorus atoms in grey. The arrows show the direction of insertion of the aminothiazol-oxyimino group.

ceftazidime side chain (Table 2, Fig. 4b). In the CTX-M-9 complex, the carboxylpropyl function interacted with the O $^{\gamma}$ atom of Ser237 and with the Arg276 side chain *via* a phosphate molecule (Table 2, Fig. 4a).⁹

The CTX-M-16 complex was superimposed on the CTX-M-9 complex,⁹ the acyl-enzyme structure of Toho-1 in complex with cefotaxime⁵ and the ultra-structure of TEM-1 in complex with the ceftazidime-like compound¹² (Fig. 5). In the Toho-1 acyl-enzyme complex, the terminal methyl function of the cefotaxime methoxyimino group is located at 3.6 Å from the C $^{\beta}$ atom of residue 237. The corresponding distance was >5 Å in CTX-M and TEM-1 in complex with ceftazidime-like compound.

The positioning of the aminothiazol-oxymino side chain in CTX-M-9 was closely related to that in the complex of TEM-1, which exhibited the worst insertion of the ceftazidime-like compound in the binding site. The ceftazidime-like compound was 0.5 to 1.0 Å more deeply inserted in the binding site of the Gly240-harboring enzyme CTX-M-16 than in those of CTX-M-9 and TEM-1, as observed for the cefotaxime adduct in the Toho-1 complex structure (Fig. 5).

Consequently, the N10 atom of the compound amide function was at van der Waals distance from the O backbone atom of residue 237 (3.4 Å) in CTX-M-9 instead to form the strictly conserved hydrogen bond observed in the Toho-1 acyl-enzyme structure with cefotaxime or in other class A complexes with glycyboronic acids.^{5,17} This last interaction was replaced by a hydrogen bond with the O $^{\gamma}$ atom of the Ser237 side chain (distance 3.1 Å). The positioning of the amide function is partially corrected in CTX-M-16; the N10 atom of the amide function is weakly closer to the O backbone atom of residue 237 than to its O $^{\gamma}$ atom (Table 2).

Molecular dynamics simulations of ceftazidime acyl-enzyme complexes

Crystallographic structures project a static view of the enzyme and only provide weak clues concerning the motions implicated in the catalytic process. The ceftazidime acyl-enzymes complexes of CTX-M-9 and CTX-M-16 were therefore modeled from crystallographic structures and analyzed by MDS. The ceftazidime acyl-enzyme structure of CTX-M-9 was designated CTX-M-9-CAZ and those of CTX-M-16, CTX-M-16S-CAZ and CTX-M-16O-CAZ, according to the positioning of the aminothiazol amino group in the direction of the solvent and the omega loop, respectively. The behaviors of these three molecular models were compared during three MDSs of 1000 ps at a temperature of 300 K. The radius of gyration and the RMSDs of C $^{\alpha}$ atoms were similar to those of the crystallographic structure of CTX-M-9 and CTX-M-16 and remained stable during the simulation (Table 3). The secondary structure was also preserved during the simulation.

The root-mean-square fluctuations (RMSFs) of the C $^{\alpha}$ atoms were, overall, similar in the three complex structures (0.64±0.32 to 0.66±0.30 Å), suggesting that the introduction of Asp240Gly did not cause a

Table 3. Summary of statistical data for MDSs

Enzyme	Radius of gyration (Å) ^a	C $^{\alpha}$ RMSD (Å) ^b	C $^{\alpha}$ RMSF (Å) ^c
CTX-M-9 crystal ^d	17.53	0.94±0.10	–
CTX-M-9-CAZ ^e	17.89±0.04	0.95±0.07	0.66±0.30
CTX-M-16 crystal ^f	17.59	0.87±0.10	–
CTX-M-16S-CAZ ^g	17.90±0.06	0.91±0.09	0.64±0.31
CTX-M-16O-CAZ ^h	17.86±0.06	1.06±0.11	0.64±0.32

^a Average radius of gyration of nonhydrogen atoms.

^b RMSD of α carbon atoms from the minimized starting structures (angstroms).

^c RMSF of α carbon atoms.

^d Crystal structure of enzyme CTX-M-9.

^e Ceftazidime acyl-enzyme structures of CTX-M-9.

^f Crystal structure of enzyme CTX-M-16.

^g Ceftazidime acyl-enzyme complex of CTX-M-16, conformation 1.

^h Ceftazidime acyl-enzyme complex of CTX-M-16, conformation 2.

global and large-scale deviation of the dynamical properties. The largest fluctuations were localized in loops connecting the secondary structure elements, as is usual in MDS (i.e., 52 to 54, 86 to 88, 111 to 114, 226 to 228, 253 to 255; RMSF=1.00±0.24 Å). The overall architectures of the active sites were similar for the three acyl-enzyme complexes. The key residues of the catalytic site (residues 70–73, 130–132, 166, and 234–237) exhibited low values of RMSFs of C $^{\alpha}$ atoms (RMSF=0.43±0.06 Å).

However, the fluctuations of residue 167 were higher for CTX-M-9-CAZ than those of CTX-M-16 acyl-enzyme complexes (0.75 for CTX-M-9-CAZ *versus* 0.44 and 0.48 Å for CTX-M-16-CAZ complexes). The behavior of residue 167 in the CTX-M-9 complex reflected a conflict between Pro167 and the bulky C7 β side-chain function of oxymino cephalosporins, which have been predicted in TEM-1 enzyme.¹⁸ This conflict was attenuated in CTX-M-16 because of the substitution Asp240Gly.

Analysis of the concerted molecular motions in ceftazidime acyl-enzyme complexes

The concerted motions in the three complexes were acquired from MDS by essential dynamics. The two principal components of these motions revealed in all simulations a bilobal flexing of CTX-M enzymes (Fig. 6). In the α domain, the conserved element number 2 (Ser130-Glu131-Asn132) and the loop harboring the residue 104 of the α structural domain moved away from the β 3 and β 4 strands of the α/β domain (Fig. 6a) and relaxed back (Fig. 6b), as the omega's residues 165, 166 and 167, suggesting that the active site is a breathing catalytic pocket composed of three lips.

Dynamic cross-correlated maps were computed from 1-ns MDSs. These maps provide details about the correlated and anticorrelated motions along the MDSs, as depicted in Fig. 7. The three acyl-enzyme complexes had an overall seemingly similar pattern. However, in the α/β domain, the motions of residues located in the β 3 and β 4 strands (amino acids 231–240 and 242–251, respectively) were more

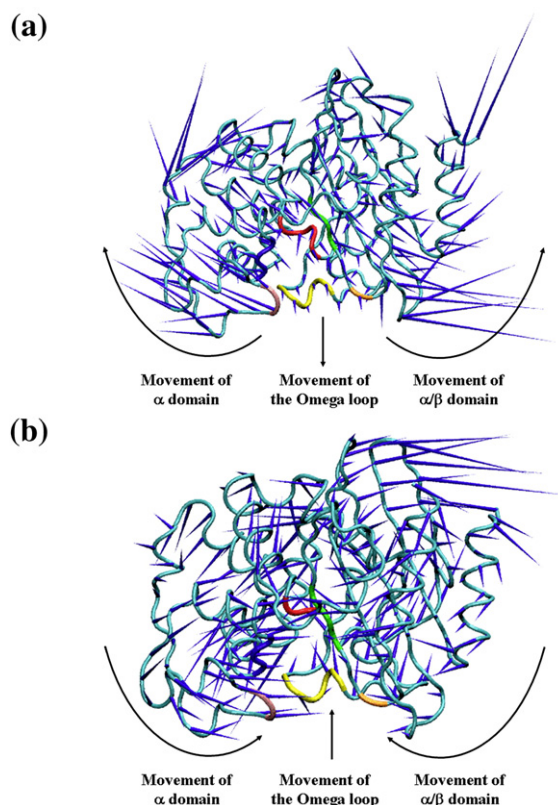


Fig. 6. Porcupine plot of principal motion of the CTX-M-9 calculated from molecular dynamics ensemble. (a) The “inspiration-like” and (b) “expiration-like” motions. The arrows show the breathing motions.

strongly coordinated for CTX-M-16-CAZ complexes than for CTX-M-9-CAZ complexes. Interestingly, the motions of residues located in the β_3 strand (positions 230 to 240) were also better coordinated with the key residues 70 (active serine of the conserved element number 1) and 167 to 170 (conserved element number 4) in CTX-M-16-CAZ than in CTX-M-9-CAZ complexes (Fig. 7).

The lifetime of hydrogen bonds between the key residues of the binding site and the ceftazidime adduct was calculated during the simulation (Table 4). The lifetime of the hydrogen bond between the ceftazidime C7 β amide function and N $^{\delta 2}$ atoms of Asn132 and Asn104 were high for all acyl-enzyme complexes ($78.0 \pm 1.1\%$ to $98.6 \pm 0.1\%$). However, the hydrogen bond between the backbone oxygen atom of residue 237 and the NH10 nitrogen atom of the ceftazidime C7 β amide group was more frequently observed in the CTX-M-16 complexes than in the CTX-M-9 complex (hydrogen lifetime, $83.6 \pm 1.3\%$ to $90.7 \pm 1.3\%$ versus $42.0 \pm 3.1\%$). This difference was suggested in the CTX-M-9 and CTX-M-16 complex structures, where the NH10 nitrogen atom was closer to the backbone O atom of residue 237 than to its O $^{\gamma}$ oxygen atom for CTX-M-16 and, conversely, for CTX-M-9 (Table 2).

A difference in behavior was also observed for the interaction between ceftazidime C3 carboxylate

function and the side chains of Thr235 and Lys234 (hydrogen bond lifetimes, $93.9 \pm 2.0\%$ to $98.9 \pm 0.4\%$ versus $54.2 \pm 6\%$). In CTX-M-16O-CAZ, the amino group of the aminothiazol ring was at hydrogen bond distance from the backbone O atom of Pro167 during 47.7% of the simulation. The substitution Asp240Gly improved, therefore, the interactions between the residues 237, 235 and the C7 β amide and C3 carboxyl groups of the substrate. The electrostatic interaction of the backbone O atom of Asn170 with the backbone N atom of the residue 240 is observed in all class A crystallographic structures. This interaction is stronger and associated with

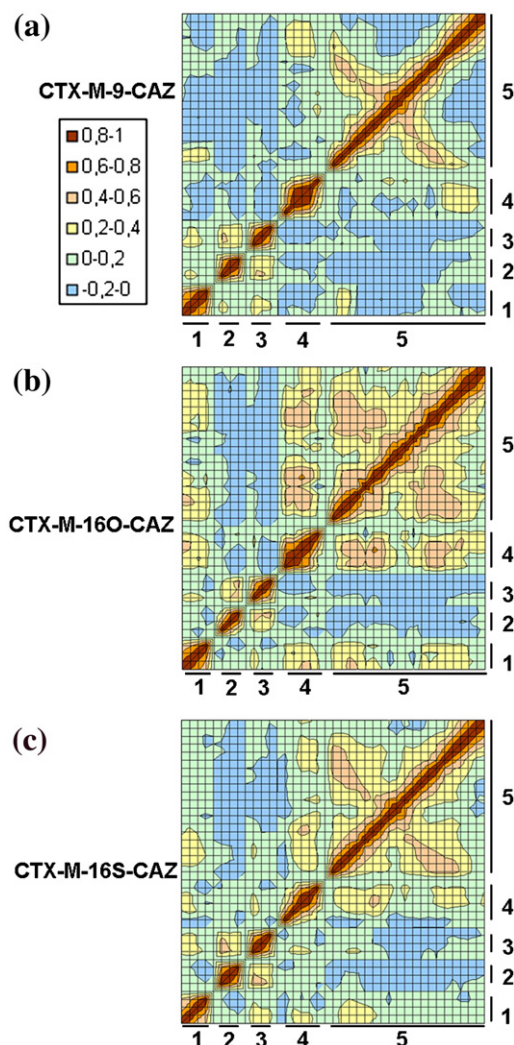


Fig. 7. The residue-to-residue dynamic cross-correlated maps for ceftazidime acyl-enzyme structures of CTX-M-9 (a, CTX-M-9-CAZ) and CTX-M-16 (b, CTX-M-16O-CAZ, and c, CTX-M-16S-CAZ). The cross-correlation maps focus on residues 70 to 73 (number 1), 104 to 106 (number 2), 130 to 132 (number 3), 166 to 170 (number 4) and 231 to 251 (the β_3 and β_4 strands, number 5). Cross-correlation coefficients ranged from -1 to $+1$. A positive value indicates a correlated movement of a residue pair, and a negative value an anticorrelated movement. The color code indicates the spectrum of correlated and anticorrelated motions from brown to blue, respectively.

Table 4. Lifetime of hydrogen bonds during MDSs of ceftazidime acyl-enzyme structures of CTX-M-9 (CTX-M-9-CAZ) and CTX-M-16 (CTX-M-16S-CAZ for conformation 1 and CTX-M-16O-CAZ for conformation 2)

Complexes	CTX-M-9-CAZ	CTX-M-16S-CAZ	CTX-M-16O-CAZ
Numbering of compound atoms			
<i>Lifetime (%) of hydrogen bonds between compound atoms and key residues of the binding site</i>			
NH10-S237O	42.0±3.1	90.7±1.3	83.6±1.3
O12-N132N δ^2	78.0±1.1	82.9±0.8	86.9±0.6
O12-N104N δ^2	88.2±2.9	97.3±0.1	98.6±0.1
O4a-T235O γ	54.2±6.0	93.9±2.0	98.9±0.4
O4a-K234N δ^1	66.8±3.5	62.8±3.1	49.8±6.1
N16a-P167O	0	0	47.7±1.9
N16a-N170O	71.6±1.2	46.0±2.0	0
<i>Lifetime (%) of hydrogen bonds between key residues of the binding site</i>			
P167O-N170N δ^2	93.3±0.4	86.0±0.6	62.5±0.7
N104O δ^1 -N132N δ^2	47.0±6.9	83.87±1.0	88.55±0.5
170O-240N	13.9±7.5	66.3±0.2	81.5±1.0

better-coordinated motions of the omega loop and the β 3 strand in CTX-M-16-CAZ complexes than in the CTX-M-9-CAZ complex.

Discussion

CTX-Ms have become dominant ESBLs in hospitals and in the community. Gly240-harboring CTX-M enzymes are particularly frequent, often associated with epidemic bacterial spreads and exhibit an unusually high activity against the key antibiotic ceftazidime. We investigated, by X-ray crystallography and molecular modeling, the accommodation of ceftazidime by the Gly240-harboring β -lactamase CTX-M-16. From this study, the mechanism for the accommodation of ceftazidime and a bilobal flexing of CTX-M enzymes emerged.

The binding site of the enzyme CTX-M-16 is not enlarged and its residue at position 240 is not able to establish electrostatic interaction with ceftazidime, in contrast to that observed with TEM- and SHV-type ESBLs.^{13,17,19} The residue Gly240 of CTX-M enzymes favored, therefore, the accommodation of the aminothiazol-oxymino side chain of ceftazidime by a different process.

Ceftazidime-like compound was deeply inserted in the binding site of the Gly240-harboring enzyme CTX-M-16, similar to the good substrate cefotaxime in the CTX-M-type enzyme Toho-1.^{5,17} In contrast, the aminothiazol-oxymino side chain of ceftazidime was only partially inserted in the binding site of CTX-M-9 and TEM-1. Ceftazidime is not hydrolyzed by TEM-1, weakly by CTX-M-9 and more efficiently by CTX-M-16.³ The insertion of oxymino adducts is therefore

correlated with the hydrolytic activity against oxymino-harboring substrates. This positioning of the adduct in CTX-M-16 favors close contacts with key residue 237 and the catalytic facilities of the enzyme, such as Glu166, which is responsible for the activation of the reactive serine 70 and the catalytic water molecule.¹¹⁻¹³ In addition, a six-member ring rocks towards the bulky oxymino group during the opening of the ceftazidime β -lactam ring (Fig. 1b). The deep insertion of the aminothiazol-oxymino side chain may prompt the accommodation of the six-member ring near the oxymino group.

MDSs were performed on the crystallographic structures to improve our understanding of substrate accommodation in the active site. These MDSs revealed a bilobal flexing of CTX-M enzymes, which leads to "inspiration and expiration motions" of the catalytic pocket (Fig. 6). The two structural domains and the omega loop of CTX-M enzymes moved away from the catalytic site during the "inspiration" and relaxed back for the "expiration." This type of motion has been previously observed with the MDM2 protein.²⁰ It may be a general behavior of proteins composed of two structural domains around a "hinge" catalytic or binding region, and favors the binding and the expulsion of ligands.

These MDSs also showed that Gly240 promotes the coordinated vibration of the β 3 strand (amino acids 230 to 240). These data agree with the anisotropic *B*-factor analyses obtained by Chen *et al.* from ultrahigh resolution.⁸ Interestingly, the motions of residues located in the β 3 strand in Gly240-harboring enzyme were also coordinated with the reactive serine 70 and residues 167 to 170 situated on the omega loop, which is critical for the accommodation of cephalosporin

acyl amide side chains in TEM-type enzymes.^{18,21} This result is explained by the location of Gly240 on the β 3 strand and the interactions of this structural element with the omega loop and the active serine 70. Consequently, these coordinated vibrations improve the canonical interactions between the residues 237 and 235 and the amide and carboxyl groups of ceftazidime.

In conclusion, the analysis of crystal structures in this work confirmed that the carboxypropyl function of the ceftazidime aminothiazol-oxymino group affects its accommodation in the active site of class A enzymes and revealed how the substitution Asp240Gly favors the accommodation of the ceftazidime side chain in CTX-M enzymes. The results support the idea that Asp240Gly substitution sparks off the enzymatic activity against ceftazidime by promoting concerted motions of key residues of the binding site.

Materials and Methods

Enzyme purification

CTX-M-16 was produced from a modified pET-9a plasmid in *Escherichia coli* BL21 (DE3). The protein was purified by ion exchange and gel filtration, as previously described.⁸

Crystal growth

Cocrystals of CTX-M-16 in complex with the glycyboronic acid were grown by vapour diffusion in hanging drops equilibrated over 1.4 M potassium phosphate buffer (pH 8.8) using microseeding techniques. The ceftazidime-like glycyboronic acid (Fig. 1a) was synthesized as previously described.²² The initial concentration of the protein in the drop was 5 mg/mL, and the concentration of the compound was 1 mM. The compound was added to the crystallization drops in a 5% dimethyl sulfoxide, 1.25 M potassium phosphate buffer (pH 8.7) solution. Crystals appeared 24–48 h after equilibration at 20 °C. Before data collection, crystals were immersed in a cryoprotectant solution of 30% sucrose and 1.8 M potassium phosphate, pH 8.8, for about 30 s, and were flash-cooled in liquid nitrogen.

Data collection and structure determination

Data were measured with a Mar-CCD detector at 100 K on the ALS beamline 8.3.1 at Lawrence Berkeley National Laboratory. Reflections were indexed, integrated and scaled using the HKL software package.²³ The space group was $P2_1$, with two molecules in the asymmetric unit. Phases were calculated by molecular replacement with the program EPMR²⁴ using the apoenzyme structure of CTX-M-9,⁹ with water molecules, and ions removed. The structure was determined to 1.80 Å resolution and refined with CNS package.²⁵ Sigma A-weighted electron density maps were calculated using CNS and used in the steps of manual model rebuilding with the program XtalView.²⁶ Cross-validation was employed throughout, and 5% of the data were used for the R_{free} calculation.²⁵ The stereochemical quality of the models was monitored with the program Procheck²⁷ and Rampage.²⁸ The figures were generated by PyMol²⁹ and Chimera.³⁰

Molecular dynamics simulation

The ceftazidime acyl-enzyme complexes were constructed on the basis of CTX-M-9 and CTX-M-16 structures in complex with ceftazidime-like boronic acid and ceftoxime.⁹ The complexes were immersed in cubic boxes filled with TIP3 water molecules.³¹ Version 1.8.2 of the VMD package was used to manipulate the systems.³² The GROMACS software package, version 3.2,³³ and the geometric and charge parameters of the OPLSAA force field³⁴ were used to carry out all energy minimizations and MDs. The particle-mesh Ewald method was used to treat long-range electrostatics.³⁵ All covalent bond lengths were constrained by the SHAKE algorithm³⁶ with a relative tolerance of 10^{-4} . After equilibration,³⁷ simulations were carried out for a total of 1000 ps. The velocities of all atoms were generated from a Maxwellian distribution. The temperature was kept constant at 300 K, while the pressure was kept constant by the weak coupling constant of 1 bar by using Berendsen's algorithms. The RMSD of backbone atoms and the thermodynamic parameters (temperature, pressure and potential energy) showed that the molecular system was equilibrated after the 200-ps MDs, and hence, the data from the last 1000 ps were used for analysis. The RMSF is the distance between the atoms of the protein structures sampled along the simulation; and the radius of gyration, a measurement of structure compactness. Two geometric criteria were used for detection of the hydrogen bond: the maximum distance between the hydrogen donor atom and the hydrogen acceptor atom was 3.2 Å; the minimum angle allowed between the hydrogen donor atom, the hydrogen atom, and the hydrogen acceptor atom was 130°. Porcupine plots of concerted motions were acquired from the three 1-ns MDs by essential dynamics³⁸ using Dynamite.²⁰

Acknowledgements

This work was supported by AORIC, PHRC du Centre Hospitalier Universitaire de Clermont-Ferrand, le Ministère Français de l'Éducation Nationale, de la recherche et de la technologie and by NIH Grant GM63813 (to B.K.S.). We thank Rolande Perroux and Marlène Jan for their technical assistance.

References

1. Knox, J. R. (1995). Extended-spectrum and inhibitor-resistant TEM-type beta-lactamases: mutations, specificity, and three-dimensional structure. *Antimicrob. Agents Chemother.* **39**, 2593–2601.
2. Matagne, A., Lamotte-Brasseur, J. & Frere, J. M. (1998). Catalytic properties of class A beta-lactamases: efficiency and diversity. *Biochem. J.* **330**, 581–598.
3. Bonnet, R. (2004). Growing group of extended-spectrum beta-lactamases: the CTX-M enzymes. *Antimicrob. Agents Chemother.* **48**, 1–14.
4. Ibuka, A., Taguchi, A., Ishiguro, M., Fushinobu, S., Ishii, Y., Kamitori, S. *et al.* (1999). Crystal structure of the E166A mutant of extended-spectrum beta-lactamase Toho-1 at 1.8 Å resolution. *J. Mol. Biol.* **285**, 2079–2087.
5. Shimamura, T., Ibuka, A., Fushinobu, S., Wakagi, T., Ishiguro, M., Ishii, Y. & Matsuzawa, H. (2002). Acyl-intermediate structures of the extended-spectrum

- class A beta-lactamase, Toho-1, in complex with cefotaxime, cephalothin, and benzylpenicillin. *J. Biol. Chem.* **277**, 46601–46608.
6. Ibuka, A. S., Ishii, Y., Galleni, M., Ishiguro, M., Yamaguchi, K., Frere, J. M. *et al.* (2003). Crystal structure of extended-spectrum beta-lactamase Toho-1: insights into the molecular mechanism for catalytic reaction and substrate specificity expansion. *Biochemistry*, **42**, 10634–10643.
 7. Shimizu-Ibuka, A., Matsuzawa, H. & Sakai, H. (2004). An engineered disulfide bond between residues 69 and 238 in extended-spectrum beta-lactamase Toho-1 reduces its activity toward third-generation cephalosporins. *Biochemistry*, **43**, 15737–15745.
 8. Chen, Y., Delmas, J., Sirot, J., Shoichet, B. & Bonnet, R. (2005). Atomic resolution structures of CTX-M beta-lactamases: extended spectrum activities from increased mobility and decreased stability. *J. Mol. Biol.* **348**, 349–362.
 9. Chen, Y., Shoichet, B. & Bonnet, R. (2005). Structure, function, and inhibition along the reaction coordinate of CTX-M beta-lactamases. *J. Am. Chem. Soc.* **127**, 5423–5434.
 10. Strynadka, N. C., Adachi, H., Jensen, S. E., Johns, K., Sielecki, A., Betzel, C. *et al.* (1992). Molecular structure of the acyl-enzyme intermediate in beta-lactam hydrolysis at 1.7 Å resolution. *Nature*, **359**, 700–705.
 11. Lamotte-Brasseur, J., Knox, J., Kelly, J. A., Charlier, P., Fonze, E., Dideberg, O. & Frere, J. M. (1994). The structures and catalytic mechanisms of active-site serine beta-lactamases. *Biotechnol. Genet. Eng. Rev.* **12**, 189–230.
 12. Minasov, G., Wang, X. & Shoichet, B. K. (2002). An ultrahigh resolution structure of TEM-1 beta-lactamase suggests a role for Glu166 as the general base in acylation. *J. Am. Chem. Soc.* **124**, 5333–5340.
 13. Nukaga, M., Mayama, K., Hujer, A. M., Bonomo, R. A. & Knox, J. R. (2003). Ultrahigh resolution structure of a class A beta-lactamase: on the mechanism and specificity of the extended-spectrum SHV-2 enzyme. *J. Mol. Biol.* **328**, 289–301.
 14. Meroueh, S. O., Fisher, J. F., Schlegel, H. B. & Mobashery, S. (2005). Ab initio QM/MM study of class A beta-lactamase acylation: dual participation of Glu166 and Lys73 in a concerted base promotion of Ser70. *J. Am. Chem. Soc.* **127**, 15397–15407.
 15. Ness, S., Martin, R., Kindler, A. M., Paetzel, M., Gold, M., Jensen, S. E. *et al.* (2000). Structure-based design guides the improved efficacy of deacylation transition state analogue inhibitors of TEM-1 beta-Lactamase(.). *Biochemistry*, **39**, 5312–5321.
 16. Murphy, B. P. & Pratt, R. F. (1988). Evidence for an oxyanion hole in serine beta-lactamases and DD-peptidases. *Biochem. J.* **256**, 669–672.
 17. Wang, X., Minasov, G. & Shoichet, B. K. (2002). Evolution of an antibiotic resistance enzyme constrained by stability and activity trade-offs. *J. Mol. Biol.* **320**, 85–95.
 18. Taibi-Tronche, P., Massova, I., Vakulenko, S. B., Lerner, S. A. & Mobashery, S. (1996). Evidence for structural elasticity of class A beta-lactamases in the course of catalytic turnover of the novel cephalosporin cefepime. *J. Am. Chem. Soc.* **118**, 7441–7448.
 19. Huletsky, A., Knox, J. R. & Levesque, R. C. (1993). Role of Ser-238 and Lys-240 in the hydrolysis of third-generation cephalosporins by SHV-type beta-lactamases probed by site-directed mutagenesis and three-dimensional modeling. *J. Biol. Chem.* **268**, 3690–3697.
 20. Barrett, C. P., Hall, B. A. & Noble, M. E. (2004). Dynamite: a simple way to gain insight into protein motions. *Acta Crystallogr., Sect. D: Biol. Crystallogr.* **60**, 2280–2287.
 21. Vakulenko, S. B., Taibi-Tronche, P., Toth, M., Massova, I., Lerner, S. A. & Mobashery, S. (1999). Effects on substrate profile by mutational substitutions at positions 164 and 179 of the class A TEM(pUC19) beta-lactamase from *Escherichia coli*. *J. Biol. Chem.* **274**, 23052–23060.
 22. Caselli, E., Powers, R. A., Blaszczak, L. C., Wu, C. Y., Prati, F. & Shoichet, B. K. (2001). Energetic, structural, and antimicrobial analyses of beta-lactam side chain recognition by beta-lactamases. *Chem. Biol.* **8**, 17–31.
 23. Otwinowski, Z. & Minor, W. (1997). Processing of X-ray diffraction data collected in oscillation mode. *Methods Enzymol.* **276**, 307–326.
 24. Kissinger, C. R., Gehlhaar, D. K. & Fogel, D. B. (1999). Rapid automated molecular replacement by evolutionary search. *Acta Crystallogr., Sect. D: Biol. Crystallogr.* **55**, 484–491.
 25. Brunger, A. T., Adams, P. D., Clore, G. M., DeLano, W. L., Gros, P., Grosse-Kunstleve, R. W. *et al.* (1998). Crystallography and NMR system: a new software suite for macromolecular structure determination. *Acta Crystallogr., Sect. D: Biol. Crystallogr.* **54**, 905–921.
 26. McRee, D. E. (1999). XtalView/Xfit—a versatile program for manipulating atomic coordinates and electron density. *J. Struct. Biol.* **125**, 156–165.
 27. Laskowski, R. A., MacArthur, M. W., Moss, D. S. & Thornton, J. M. (1993). PROCHECK: a program to check the stereochemical quality of protein structures. *J. Appl. Crystallogr.* **26**, 283–291.
 28. Lovell, S. C., Davis, I. W., Arendall, W. B., 3rd, de Bakker, P. I., Word, J. M., Prisant, M. G. *et al.* (2003). Structure validation by C α geometry: phi,psi and C β deviation. *Proteins*, **50**, 437–450.
 29. DeLano, W. L. (2002). The PyMOL molecular graphics system on the World Wide Web, <http://www.pymol.org>.
 30. Pettersen, E. F., Goddard, T. D., Huang, C. C., Couch, G. S., Greenblatt, D. M., Meng, E. C. & Ferrin, T. E. (2004). UCSF Chimera: a visualization system for exploratory research and analysis. *J. Comput. Chem.* **25**, 1605–1612.
 31. Jorgensen, W., Chandrasekhar, J., Madura, J. & Klein, L. (1983). Comparison of simple potential functions for simulating liquid water. *J. Chem. Phys.* **79**, 926–935.
 32. Humphrey, W., Dalke, A. & Schulten, K. (1996). VMD: visual molecular dynamics. *J. Mol. Graphics*, **14**, 33–38, 27–28.
 33. Lindahl, E., Hess, B. & van der Spoel, D. (2001). GROMACS 3.0: a package for molecular simulation and trajectory analysis. *J. Mol. Model.* **7**, 306–317.
 34. Jorgensen, W. L., Maxwell, D. S. & Tirado-Rives, J. (1996). Development and testing of the OPLS all-atom force field on conformational energetics and properties of organic liquids. *J. Am. Chem. Soc.* **118**, 11225–11236.
 35. Darden, T., York, D. & Pedersen, L. (1993). Particle mesh Ewald—an $N \log(n)$ method for Ewald sums in large systems. *J. Chem. Phys.* **98**, 10089–10092.
 36. Ryckaert, J., Ciccotti, G. & Berendsen, H. (1977). Numerical integration of the Cartesian equations of motion of a system with constraints: molecular dynamics of n -alkanes. *J. Chem. Phys.* **23**, 327–341.
 37. Maveyraud, L., Golemi-Kotra, D., Ishiwata, A., Meroueh, O., Mobashery, S. & Samama, J. P. (2002). High-resolution X-ray structure of an acyl-enzyme species for the class D OXA-10 beta-lactamase. *J. Am. Chem. Soc.* **124**, 2461–2465.
 38. Amadei, A., Linssen, A. B. & Berendsen, H. J. (1993). Essential dynamics of proteins. *Proteins*, **17**, 412–425.